Cargo-Towing Fuel-Free Magnetic Nanoswimmers for Targeted Drug Delivery

Wei Gao, Daniel Kagan, On Shun Pak, Corbin Clawson, Susana Campuzano, Erdembileg Chuluun-Erdene, Erik Shipton, Eric E. Fullerton, Liangfang Zhang, Eric Lauga,* and Joseph Wang**

***F**uel-free nanomotors are essential for future in-vivo biomedical transport and drug-delivery applications. Herein, the first example of directed delivery of drug-loaded magnetic polymeric particles using magnetically driven flexible nanoswimmers is described. It is demonstrated that flexible magnetic nickel–silver nanoswimmers (5–6 μm in length and 200 nm in diameter) are able to transport micrometer particles at high speeds of more than 10 μm s^{-1} (more than 0.2 body lengths per revolution in dimensionless speed). The fundamental mechanism of the cargo-towing ability of these magnetic (fuel-free) nanowire motors is modelled, and the hydrodynamic features of these cargo-loaded motors discussed. The effect of the cargo size on swimming performance is evaluated experimentally and compared to a theoretical model, emphasizing the interplay between hydrodynamic drag forces and boundary actuation. The latter leads to an unusual increase of the propulsion speed at an intermediate particle size. Potential applications of these cargo-towing nanoswimmers are demonstrated by using the directed delivery of drug-loaded microparticles to HeLa cancer cells in biological media. Transport of the drug carriers through a microchannel from the pick-up zone to the release microwell is further illustrated. It is expected that magnetically driven nanoswimmers will provide a new approach for the rapid delivery of target-specific drug carriers to predetermined destinations.*

W. Gao,[+] D. Kagan,[+] Dr. C. Clawson, Dr. S. Campuzano, E. Chuluun-Erdene, Dr. E. Shipton, Prof. E. Fullerton, Prof. L. Zhang, Prof. J. Wang
Department of Nanoengineering
University of California
San Diego, La Jolla, CA 92093-0448, USA
E-mail: zhang@ucsd.edu; josephwang@ucsd.edu
O. S. Pak, Prof. E. Lauga
Department of Mechanical and Aerospace Engineering
University of California
San Diego, La Jolla CA 92093-0411, USA
E-mail: elauga@ucsd.edu
[+] These authors contributed equally to this work.

DOI: 10.1002/smll.201101909

1. Introduction

The proper understanding and execution of nanomotor biological functionality, i.e., pick-up, transport, and delivery of biologically relevant nanostructured loads,[1–9] is crucial for myriad future biomedical applications including drug delivery and gene therapy. Past work from both Sen's group and our team has previously demonstrated the ability of catalytic nanowire motors to pick up, tow, and release spherical polystyrene particles.[1,2] Our group has also recently demonstrated the guided transport of drug-loaded liposomes,[3] pancreatic cancer cells,[10] and nucleic acids[11] by fuel-driven nanomotors. Despite these advances in cargo-towing by catalytic nanomotors, future ex-vivo and in-vivo biomedical

NANO MICRO small

transport applications require the use of biocompatible, fuel-free nanomotors.

In this work, we describe the efficient cargo-towing capabilities of magnetically driven (fuel-free) nanomotors, elucidate the fundamental mechanism of cargo-towing by these flexible nanoswimmers, and assess to what extent they can be used to transport relevant cargo in biological media. Magnetically driven nanomotors, which swim under externally applied magnetic fields, are particularly promising for use in a variety of biomedical applications,[9,12,13] as they can perform complex manoeuvres while obviating fuel requirements. To examine the directed transport of payloads by these fuel-free magnetic swimmers, we rely here on our recently developed flexible nanowire motors that are prepared by a templated electrodeposition approach.[14–16] These two- or three-segment, flexible nanowire motors consist of a rotating magnetic nickel head (≈1.5 μm long), along with a flexible silver segment (≈4 μm long). These swimmers appear to be among the fastest fuel-free synthetic nanomotors reported to date in terms of dimensionless swimming speed (obtained by dividing the dimensional speed, by the body length, and the actuation frequency, to scale off the effects of motor size and frequency), allowing them to propel efficiently in biological fluids.[16] Despite the great potential for these magnetically propelled nanoswimmers in diverse biomedical applications, their ability to carry a cargo has not yet been demonstrated.

In order to elucidate the fundamental mechanisms of cargo-towing by flexible magnetic nanomotors, we examine the transport of various-sized, drug-loaded magnetic polymeric microspheres made of pol(D,L-lactic-*co*–glycolic acid) (PLGA). We investigate their towing performance and discuss the hydrodynamic features of these cargo-loaded motors. The effect of the iron oxide-loaded cargo size upon the swimming performance is evaluated experimentally and compared to a theoretical model, emphasizing the interplay between hydrodynamic drag forces and boundary actuation. The performance of these new fuel-free nanowire motors makes them attractive for future biomedical applications, as illustrated below for the directed delivery of drug-loaded microparticles to HeLa cells in cell-culture media. Our investigations will ultimately enable us to address the performance and physical limitations of nanomotor towing for the efficient transport of biological and therapeutic payloads.

2. Results and Discussion

2.1. Cargo-Towing Magnetic Nanowire Motors

Figure 1a–f shows a sequence of pictures, taken at 20 ms intervals, of the motion of a magnetic nanowire motor carrying a ≈1.0 μm drug-loaded magnetic PLGA microsphere under a rotating magnetic field (the magnetic moment of the microsphere arises due to the encapsulation of iron oxide nanoparticles); see the Supporting Information (SI) Figure 1 for the magnetic field setup. These images were taken from the corresponding video (SI, Supporting Video S1) that displays the entire movement of the sphere-loaded flexible nanoswimmer. As clearly seen in this video, the motor rotates around the cargo

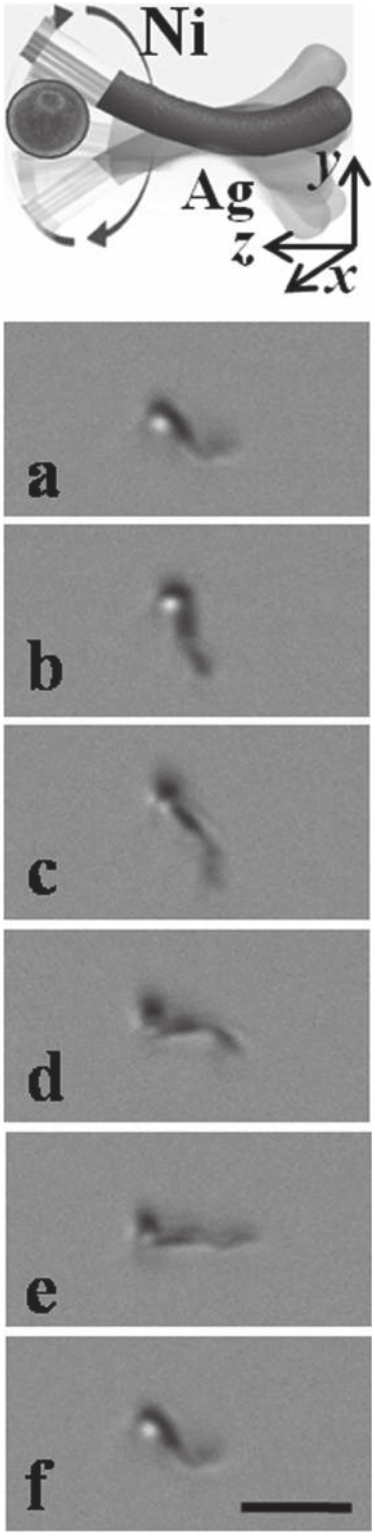

Figure 1. Time-lapse images, taken from Video S1 in the SI, depicting the slow motion of a magnetic nanowire motor with a 1.0 μm drug-loaded magnetic PLGA microsphere. The time interval between each image is 20 ms. Scale bar 5 μm. Magnetic field: $f = 10$ Hz, $H_1 = 10$ G, and $H_0 = 9.5$ G.

(the particle is loaded inside the cone swept by the nickel), which is further shown by the disappearance of the particle during each rotation cycle. The location of the magnetic cargo

towards the free end of the nickel segment also confirms that the particle is magnetically bound, as the nickel segment's poles are the strongest attraction points. The motor is actuated by the magnetic nickel segment, which follows closely the external rotating magnetic field. Through boundary actuation, the flexible silver filament deforms in a chiral fashion to produce propulsion in the direction towards the nickel segment. The necessity of chirality in the deformation for propulsion was established in our previous work, together with a simple elastohydrodynamic model for its propulsion.[16] Using high-definition images from the video, we noticed that the deformation of the flexible filament does not seem to change significantly after picking-up the cargo sphere. The deformation of the silver segment is very apparent in the slow-motion video frames, which show the segment whipping and driving the propulsion of the cargo-carrying wire through the fluid. The exact shape of the silver filament is a result of the competition from magnetic actuation, elastic forces from the flexible filament, and viscous forces from the fluid medium.[16] Overall, these results demonstrate that our flexible magnetic nanoswimmers are able to transport micrometer particles at high speeds, both dimensional (up to 10 μm s^{-1}) and dimensionless (up to 0.2 body lengths per revolution).

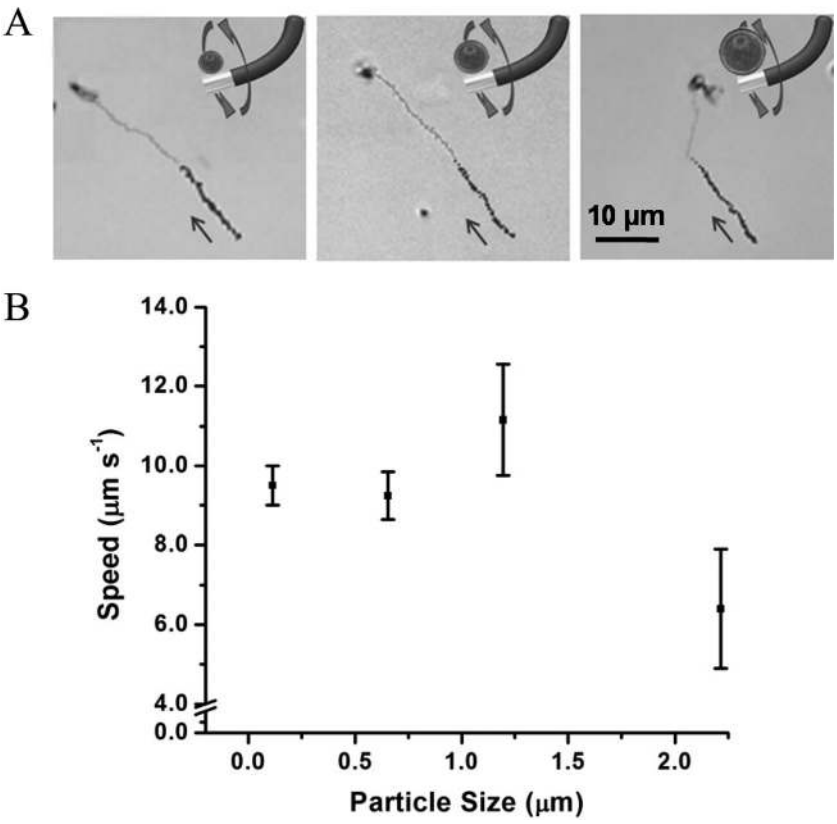

Figure 2. A) Capture and transport of different sizes of drug-loaded magnetic PLGA micro/nanoparticles. Time-lapse images (corresponding to SI, Video S2) showing the motion trajectory within 2 s before and after picking up the different-sized, drug-loaded PLGA particles, respectively. B) Variation of the speed of the magnetic nanowire motors after picking up different sizes of drug-loaded PLGA particles. Error bars estimated as a triple of the standard deviation (n = 20). Magnetic fields as in Figure 1.

The picking up of polymeric magnetic particles of distinct, different sizes (radii ranging from 500 nm to 2.5 μm) was used to assess the influence of cargo size on the nanomotors' speed and trajectory. **Figure 2**A shows actual optical images highlighting the directed motion of the magnetic nanomotor towards a drug-loaded PLGA particle, followed by the instantaneous capture of a magnetic polymeric sphere by the nanomotor and its transport. This cargo loading is accomplished via the magnetic attraction between the nickel segment on the nanomotor and the iron oxide nanoparticles encapsulated in the PLGA particle. Video S2 (in the SI) depicts the progression of events featured in Figure 2 for three PLGA cargo spheres, representative of different particle-size groups (of average diameters 0.65, 1.25, and 2.25 μm). As was illustrated in our previous work,[16] the magnetic frequency and strength have a profound influence on the speed of nanoswimmer, and should thus influence its cargo-towing ability.

In previous studies on cargo transportation using catalytic fuel-driven nanomotors,[1–3] loaded particles were found to increase the hydrodynamic resistance, and led to a monotonic decrease in propulsion speed with particle size. Upon loading, the hydrodynamic center changes only along the axis of the nanowire; since the motion of the catalytic motor is only along the axial direction, the loading process simply contributes additional hydrodynamic drag to the motor. The additional loading obeys Stokes' law for the viscous resistance of spheres (the force (F) to speed (U) ratio is given by $F/U = 6\pi\mu a_r = R_s a_r$ where a_r is the dimensional radius of the sphere, R_s is $6\pi\mu$, and μ is the fluid viscosity) and results in a monotonic decrease in propulsion speed upon increasing the size of the loaded particle.

In contrast, here, we observe an unusual nonmonotonic impact of the cargo loading on the speed and trajectory of the magnetic nanowire motors. As shown in Figure 2B, for the small drug-loaded particles (average diameters of 0.2 and 0.65 μm), the cargo-loaded nanomotors travel at approximately the same speed (9.5 μm s^{-1}) as before the loading; for the medium size of cargo (average diameter of 1.25 μm), we observed an unexpected (≈20%) increase in the propulsion speed after pick-up; however, a significant reduction in the average speed (≈33%) was observed for the very large particle (average diameter of 2.25 μm). In the following sections we attempt to rationalize the physical basis for this nonmonotonic velocity change.

2.2. Dynamic Considerations

An investigation into the magnetic contribution added by the iron oxide-loaded particles to the magnetic nickel segment

NANO MICRO small

of the motor reveals that the particle's magnetic moment is several orders of magnitude smaller than that of the nickel segment. The magnetic torque on the nickel segment still dominates the motion, and hence the slope of the nickel segment is still slaved to that of the external magnetic field (small Mason number limit, given by the ratio of viscous-to-magnetic forces). The observed nonmonotonic propulsion is therefore not attributed to the extra magnetic moment introduced by the particle whose sole effect is to allow for the attachment of the particle to the nanomotor.

Since the particle is attached to the nickel segment via magnetic attraction, the rotation of the nickel segment leads to spinning of the particle cargo at the same rate. Therefore, the presence of the particle not only contributes additional viscous drag but also sets up a rotating flow field due to its spinning motion. Can the flow field induced by the spinning particle influence the propulsion velocity? We answer this question by extending the calculations of reference [16] while also including a background flow field generated by the spinning particle of radius a_r, placed immediately next to the silver filament (sphere centered at $z = L + a_r$, hence maximum influence). We nondimensionalized lengths and time by using the silver filament's length, L, and the inverse of the angular frequency, $1/\Omega$, respectively. Details of the derivation are included in the Supporting Information. Expanding the deformation and swimming velocity in powers of h (ratio of the amplitude of the transverse and longitudinal magnetic fields), we have $\vec{r}_\perp(z) = h\,\vec{r}_{\perp 1}(z) + h^2\,\vec{r}_{\perp 2}(z) + \cdots$ and $U = h\,U_1 + h^2\,U_2 + \cdots$. The first-order deformation $\vec{r}_\perp = [x(z), y(z)]$ is governed by the dimensionless equations

$$-y\left[1-\left(\frac{a}{1+a-z}\right)^3\right] = Sp^{-4}\frac{d^4x}{dz^4} \quad (1)$$

$$x\left[1-\left(\frac{a}{1+a-z}\right)^3\right] = Sp^{-4}\frac{d^4y}{dz^4} \quad (2)$$

where $a = a_r/L$ is the dimensionless radius of the sphere, and the sperm number $Sp = L(\xi_\perp \Omega/A)^{1/4}$ is a dimensionless parameter comparing the viscous to elastic forces ($\xi_\perp$ is the drag coefficient of a slender filament moving perpendicular to its axis and A is the bending stiffness of the filament).[17,18] In the absence of the sphere ($a = 0$), the above equations reduce to the case of an unloaded motor.[16] We apply the boundary conditions $\partial^3\vec{r}_\perp/dz^3(z=0) = \partial^2\vec{r}_\perp/dz^2(z=0) = 0$ and $x(z=1) = b = 0$, $y(z=1) = \partial y/\partial z(z=1) = 0$ and $\partial x/\partial z(z=1) = 1$ as in reference [16], where b represents the displacement of the Ni–Ag junction. Balancing the $O(h)$ local viscous force in the longitudinal direction yields $U_1 = 0$, so swimming occurs at $O(h^2)$. Upon solving for $(x_1(z), y_1(z))$, we obtain the second-order swimming velocity of the nanomotor, U_2 (refer to SI for details). Next, we compare in **Figure 3** the case when there is no particle ($a = 0$, solid line) and when there is a large particle (2.5 μm in diameter, $a = 0.3125$, dashed line). It is observed that the effect of the flow field set-up by the spinning sphere acts to reduce the propulsion speed for all sperm numbers. For a large particle of diameter 2.5 μm, the maximum reduction in speed due to the flow field is around

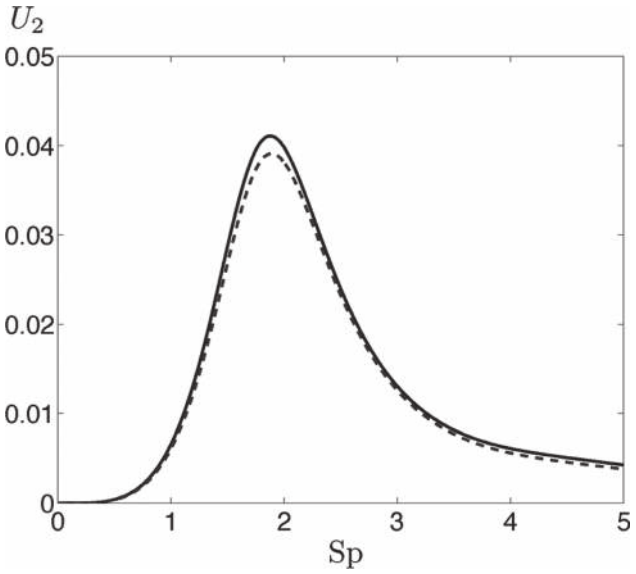

Figure 3. Dimensionless second-order propulsion speed, $U/L\,\Omega = h^2 U_2 + O(h^3)$, as a function of the sperm number (Sp) for the case when there is no particle ($a = 0$, solid line) and when there is a large particle of diameter 2.5 μm ($a = 0.3125$, dashed line).

5%. For even larger particles (5 μm in diamater), the reduction is at most 16%, while experimentally we observed no apparent propulsion for larger size of particles. Therefore, for the size of particles considered in the experiments, this effect is negligible.

The nonmonotonic variation of the swimming speed is actually caused by a subtle change, brought about by the loading process, in the boundary condition for the filament actuation. Unlike catalytic motors, the attachment of a spherical particle to the magnetic nickel segment of the current motor not only increases the viscous drag, but also perturbs the total force and torque balances, which in general lead to a change in the boundary actuation conditions (the displacement and slope at $z = 1$, the Ni–Ag junction) and hence the deformation of the entire silver filament. Since the propulsion speed is a function of the shape of the silver filament, a nontrivial modification to the propulsion speed is expected. The slope at the boundary is still slaved to the external magnetic field, but we believe that the location of the hinge (the point about which the filament rotation occurs) is displaced by the attachment of the particle. Consider first a simplified scenario for illustrative purposes. Upon the action of a planar rotating magnetic field, a rigid magnetic nanowire of unit length should rotate about its mid-point symmetrically, to maintain an overall force-free condition (**Figure 4** inset A, left panel). Now imagine the center of a spherical particle of radius a (dimensionless) attached to one end of the nanowire. One would expect the rotation point to shift towards the side with the attached particle (denoted b_s) to maintain the force-free condition (Figure 4 inset A, right panel). A simple force balance reveals that $b_s = a\beta/2(1+a\beta)$ for this scenario, where $\beta = R_s/\xi_\perp$. For this reason, the attachment of a cargo particle to the nanowire motor in the experiment changes the location of the point of rotation, which is approximately located at the

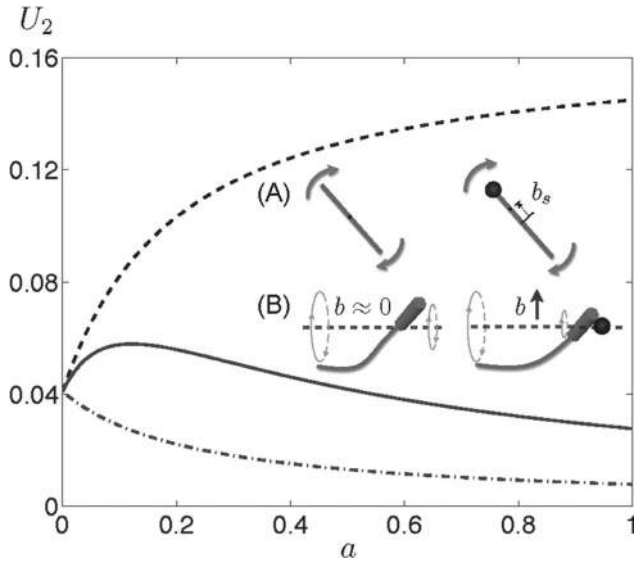

Figure 4. Dimensionless second-order propulsion speed, $U/L\,\Omega = h^2 U_2 + O(h^3)$, as a function of the dimensionless particle radius. Dashed curve: the isolated effect of the change in boundary conditions, $x(z=1) = -a\beta \sin\theta/2(1+a\beta)$, without the effect of additional hydrodynamic resistance from the particle; dot-dashed curve: the effect of the additional hydrodynamic resistance from the particle, without change in boundary conditions, $x(z=1) = 0$; solid curve: the combined effect of the change in boundary actuation conditions and the extra hydrodynamic resistance from the particle. Inset (A): the simplified scenario of a planar rotation of a nanowire, illustrating the shift of rotation center upon the attachment of a spherical particle. Inset (B): schematic illustration of the possible change in boundary actuation condition upon particle loading.

Ni–Ag junction before loading, hence $b \approx 0$ (Figure 4 inset B, left panel). In order to maintain the force-free condition, the point of rotation is expected to shift towards the location where the cargo is attached. Hence, an increase in the magnitude of b in the boundary actuation is anticipated (Figure 4 inset B, right panel). A detailed numerical simulation including all the hydrodynamic interactions and the effect of the surface is required to determine the exact value of b. To illustrate qualitatively the possible effect of such a change, we use the expression of the simplified scenario described above and scale it by $\sin\theta$ (where θ is the angle made by the resultant magnetic field with the constant magnetic field) as a rough estimation for the value of the boundary condition, i.e., $x_1(z=1) = -b_s \sin\theta$. In Figure 4, we illustrate different effects separately. We first assume that the loading process amounts to no change in the boundary actuation condition, and show only the effect of the additional viscous drag from the particle. As expected from Stokes law for a sphere, the speed of the motor deceases monotonically with the size of the attached particle (dash-dotted curve). Next, we ignore the increased hydrodynamic resistance from the sphere and observe the effect of the change in boundary actuation described above: $x_1(z=1) = -a\beta \sin\theta/2(1+a\beta)$. Such a change in the boundary condition tends to monotonically enhance the propulsion speed nonlinearly, as shown by the dashed line. The combined effect of the change in boundary actuation conditions and the extra hydrodynamic resistance from the particle produces a nonmonotonic variation of the propulsion speed with particle size (solid curve). For small-to-medium-sized loaded particles, the propulsion speed can indeed be enhanced after loading. However, for very large particles, the increase in hydrodynamic resistance dominates and reduces the propulsion speed. This simple analysis suggests a possible mechanism for the counter-intuitive increase in propulsion upon loading shown in Figure 2. Since the boundary conditions employed are obtained from a simplified geometry and hydrodynamic interactions could also be important in this scenario,[19] we do not expect a quantitative agreement bewteen theory and experiment. Instead we aim to suggest a possible mechanism capturing qualitively this nonmonotonic feature of cargo loading.

For large particles (≈2 μm in diameter), in addition to the 30% reduction in speed, we also observed a significant change in the motor trajectory after loading. For unloaded motors, or when the loading particle is small, the motor propels in the direction of the axial magnetic field both before and after the loading (Figure 2A, left and middle panel). However, when the cargo is large, the new trajectory is seen to occur at an angle with respect to the axial magnetic field (Figure 2A, right panel). Such a change in the cruising angle could be attributed to hydrodynamic interactions with surfaces, which is expected to play a more significant role when the loading particle is large. The presence of a surface breaks spatial symmetry and the viscous drag experienced by a moving body is higher when located close to the bottom surface. Tierno et al. first exploited this type of drag anisotropy in order to convert the rotational motion of an anisotropic colloidal doublet (i.e., a small sphere attached to a larger sphere) near a surface into translational motion.[20,21] As pointed out in their work, the higher viscous drag near the surface plays a role similar to the solid friction between a rolling wheel and a solid surface. When loaded with a particle, our current nanowire motor is geometrically similar to an anisotropic doublet, and hence we suspect that the off-axis propulsion velocity after loading is due to a similar mechanism. The current nanowire motor performs thus both as a flexible propeller (propelling in the direction of the constant magnetic field) and as a surface walker (propelling in a direction perpendicular to the constant magnetic field) when it is loaded with a large particle in the presence of a surface. For future applications close to a surface/boundary and requiring a preservation of the cruising direction, the cargo particle has therefore to be limited in size to avoid any interference with the swimming direction of the motor.

2.3. Targeted Drug Delivery

The results obtained through the former study illustrate that the iron oxide-loaded polymeric particles and the size of the nickel segment within the nanomotors are sufficient for enabling the particle's pick-up and transport. These results also demonstrate that the size of the drug-loaded spheres plays a significant role in the speed and trajectory of the cargo-loaded Ni–Ag nanowire motors. After having studied the physicochemical properties and cargo-carrying capability of

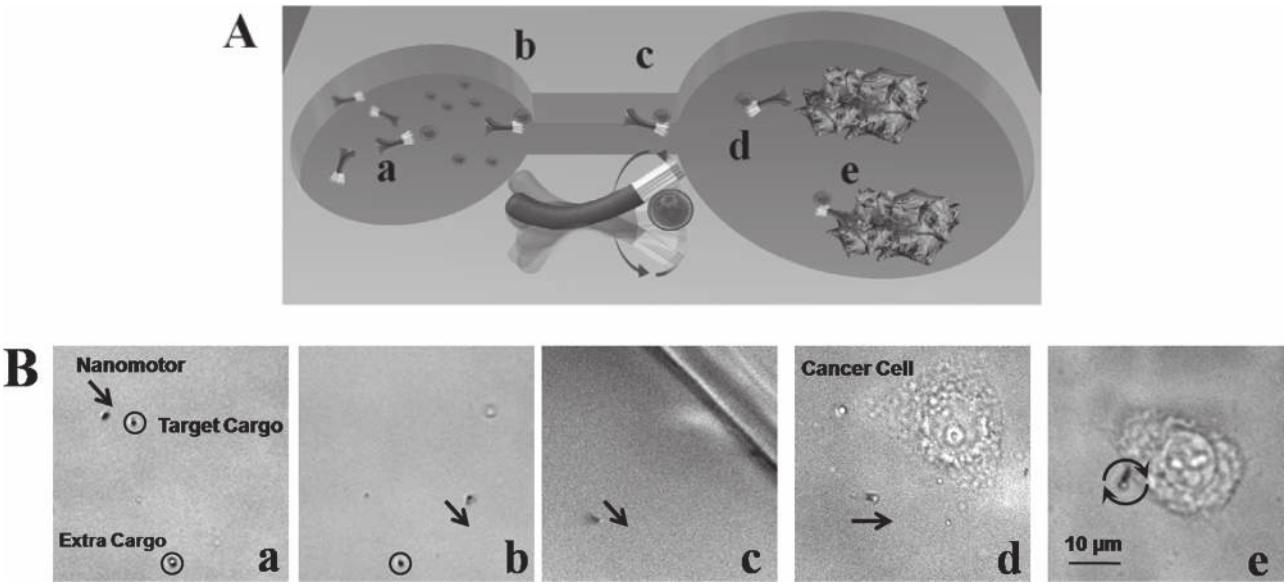

Figure 5. Drug delivery to HeLa cells using flexible magnetic nanoswimmers in cell-culture media. A) Scheme depicting the process as a flexible magnetic Ni–Ag nanowire motor (a); captures the drug-loaded magnetic polymeric particle in the loading reservoir (b); transports it through the channel (c); approaches the target cell (d); sticks onto the target cell, and releases the drug (e). B) Time-lapsed images illustrating each of the previous described steps, taken from Video S3 (SI). The arrows show the moving direction of the nanoswimmer. Conditions as in Figure 1.

the magnetic nanoswimmers, we next examine the potential practical utility of these fuel-free nanomotors by experimentally delivering drug (e.g., doxorubicin)-loaded PLGA microparticles to cancer cells in an in-vitro setting. This active transport, which usually occurs at a rate orders of magnitude faster than diffusion,[3] takes place through a microchannel that connects the pick-up zone to the release microwell, as illustrated schematically in **Figure 5**A. The corresponding experimental results are shown in Figure 5B (corresponding to the SI, Video S3). For systemic drug-delivery purposes, most drug carriers (e.g., PLGA particles and liposomes) are used at a sizes smaller than 1 μm, where the flexible nanomotors do not have any obvious speed changes. In this study, in order to directly visualize the concept of delivering drug-loaded particles to target cancer cells, we used PLGA particles of around 1.25 μm in size. Experiments were conducted using HeLa cancer cells because they can readily adhere to the plasma-treated glass wells when incubated overnight in a culture medium. Repeatedly washed, flexible nanowire motors and drug-loaded PLGA particles were added to a culture medium solution in the left well and the cancer cells were seeded and cultured in the right well. Figure 5 shows both a cartoon (panel A) and captured experimental images of a five-step in-vitro process, which is used to emulate the fuel-free motors drug delivery capabilities (panel Ba–e). First, the flexible nanomotor approaches the target iron oxide/doxorubicin-encapsulated PLGA particle in a cell-free well via precise magnetic guidance (point marked 'a'). As the motor passes close by the particle, the particle is magnetically attracted and picked up (point 'b'). The long-range transport capability of the flexible nanomotor is then tested while it tows and guides the PLGA particle across the channel ('c') and to the open secondary well containing the HeLa cancer cells. The nanomotor is then guided to a target HeLa cancer cell ('d'), which is attached and spread across the bottom surface. Finally, the flexible silver segment of the nanowire nonspecifically bound to the HeLa cell to enable localized drug release from the PLGA particle ('e'). We observed this nonspecific binding several times when the motor was directed to the cancer cell and given enough time to interact. In most cases the cargo-loaded nanomotor tended to travel around or over the cell as it perpetually interacted with the cellular membrane. Future endeavors could involve nanomotors functionalized with antibodies specific to cancer cells, to increase their binding efficiency once they have been directed to the target cells. This nanomotor-based, targeted, drug-delivery system involving fuel-free nanovehicles may potentially address current challenges of nanoparticle drug delivery, such as inevitable off-targeting of particles and the likelihood of systemic toxicity.

3. Conclusion

In conclusion, we demonstrated the first example of directed transport of magnetic polymeric drug carriers by fuel-free flexible magnetic nanomotors, investigated both experimentally and theoretically the influence of such cargo upon the propulsion speed and trajectory of the loaded motor, and elucidated the fundamental mechanism of such cargo towing. These fuel-free nanomotors have been shown useful for the pick-up and transport of various drug carriers from a loading zone to a predetermined destination through a predefined route, and they represent a novel approach towards transporting cargos in a target specific manner. Note that the transport occurs at a rate order of magnitude faster than that expected from Brownian motion. The new understanding will ultimately enable us to address the performance and physical limitations of nanomotor-towing for the efficient transport of biological and therapeutic payloads.

Despite these significant advancements of nanomotor design and our new understanding of the ability of the flexible nanoswimmer to transport cargo, several challenges still exist for their practical in-vivo use. Enhancements on the propulsive thrust and cargo attachment are necessary to overcome any additional hydrodynamic drag and shear present in the in-vivo environment. To further improve the efficiency of nanomotor-based drug delivery, we envision the possibility of attaching drug carriers to these magnetically driven nanoswimmers through cleavable linkers that are responsive to tumor microenvironments (e.g., enzymes and acidic pH) to enable an autonomous release of the carriers and a more accurate delivery of cargos to the target site. While eliminating the fuel requirements, attention must be given also to the preparation of more biocompatible magnetic nanowimmers. Eventually, such magnetically driven fuel-free nanoswimmers are expected to provide a new and unique approach for rapidly delivering drug carriers to predetermined destinations in a target-specific manner.

4. Experimental Section

Reagents and Solutions: Cupric sulfate pentahydrate, nickel(II) chloride hexahydrate, nickel(II) sulfamate tetrahydrate, gold (Orotemp 24 RTU RACK) and silver (1025 RTU @ 4.5 Troy/gallon) plating solutions were purchased from Technic Inc., Anaheim, CA. All chemicals used were of analytical-grade reagents, and deionized water was obtained from a Millipore Milli-Q purification system (18.2 MΩ cm). For the preparation of the drug-loaded magnetic PLGA microparticles, doxorubicin hydrochloride (Sigma-Aldrich), triethylamine (Sigma-Aldrich), dichloromethane (Sigma-Aldrich), PLGA-ester (50:50 lactic acid: glycolic acid, IV 0.82 dL g^{-1} from Lactel, Pelham, AL), oleic acid-coated 10 nm Fe_3O_4 nanoparticles (OceanNanoTech; Fayetteville, AR), polyvinyl alcohol (PVA, MW 85000, 80% hydrolyzed, Sigma-Aldrich) and centrifuge filters (Amicon, 100 kDa MW cut-off (MWCO)) were used. Standard White Polycarbonate 'Track Etch' Membrane Filters from SPI-Pore were used to obtain different size of microparticles. A commercial Sylgard 184 Silicone elastomer kit (Dow Corning Corporation, Midland, MI) was used for the preparation of the PDMS channel (see below).

For the HeLa cell-culture RPMI (Roswell Park Memorial Institute) medium, fetal calf serum, penicillin, streptomycin, and trypsin, all purchased from Life Technologies (Carlsbad, CA), were used.

Apparatus: Template electrochemical deposition of nanowires was carried out with a CHI 660D potentiostat (CH Instruments, Austin, TX). An inverted optical microscope (Nikon Instrument Inc. Ti-S/L100), coupled with a 40× objective, a Photometrics QuantEM 512/SC camera (Roper Scientific, Duluth, GA) and a MetaMorph 7.6 software (Molecular Devices, Sunnyvale, CA) were used for capturing movies. The video for Figure 1 was captured using a Hamamatsu digital camera C11440, 40× objective and was acquired at the frame rate of 100 fps using the NIS-Elements AR 3.2 software.

Synthesis of Flexible Ni–Ag_{flex} Magnetic Nanowires: The nanowire motors were prepared using a common template-directed electrodeposition protocol.[14–16] A silver film was first sputtered on one side of the porous alumina membrane template containing 200 nm-diameter cylindrical pores (Catalog No 6809-6022; Whatman, Maidstone, UK) to serve as a working electrode. The membrane was then assembled in a plating cell with an aluminum foil serving as a contact for the sputtered silver. Copper was electrodeposited in the 'branch' area of the membrane from a $CuSO_4 \cdot 5H_2O$ (1 M) solution, using a charge of 8 C and a potential of –0.9 V (versus an Ag/AgCl reference electrode, along with a Pt wire counter electrode); subsequently, gold was plated next from the commercial gold plating solution at -0.9 V (versus Ag/AgCl), using a charge of 0.5 C, which was used for protecting the nickel while dissolving the membrane later; nickel was deposited from a nickel-plating solution containing $NiCl_2 \cdot 6H_2O$ (20 g L^{-1}), $Ni(H_2NSO_3)_2 \cdot 4H_2O$ (515 g L^{-1}), and H_3BO_3 (20 g L^{-1}) at –1.0 V (versus Ag/AgCl) for 6 C; finally, silver was plated at –0.9 V (versus Ag/AgCl) for a total charge of 4.5 C using a commercial silver-plating solution. The sputtered silver layer was mechanically removed from the membrane by polishing with alumina particles (3–4 μm); the sacrificial copper layer was dissolved using a 20% HCl solution containing 0.5 M $CuCl_2$. The membrane was then dissolved in a NaOH (3 M) solution for 30 min to completely release the nanowires. The nanowires were collected by centrifugation at 6000 rpm for 5 min and were washed repeatedly with nanopure water (18.2 MΩ cm) until a neutral pH was achieved. All nanowire solutions were stored in nanopure water at room temperature. Flexibility of the silver segment was achieved by its partial dissolution accomplished by mixing the diluted Ni–Ag nanowire solution (10 μL) with the hydrogen peroxide solution (10% (w/v), 10 μL) for 1 min. The nanowires were then washed on the glass slides using nanopure water (18.2 MΩ cm) until a neutral pH was achieved. The resulting nanomotors had a single rigid 1.5 μm-long Ni segment, a 4 μm-long flexible silver segment and a 0.3 μm-long gold segment (for protecting the Ni), giving a total nanowire length of 5.8 μm.

Preparation of the Drug-Loaded, Magnetic PLGA Microparticles: Doxorubicin-loaded magnetic PLGA microparticles were prepared using an oil-in-water emulsion method.[22] Briefly, an excess of triethylamine was added to an aqueous solution of doxorubicin hydrochloride in order to neutralize the hydrochloride ion. The resulting free-base doxorubicin was extracted from the aqueous solution with dichloromethane. The extraction was performed three times to improve yield. The collected free-base doxorubicin was dried under argon and dissolved in chloroform at 1 mg mL^{-1}. Meanwhile, PLGA–ester (10 mg, 30 mg mL^{-1}, 50:50 lactic acid: glycolic acid, IV 0.82 dL g^{-1} from Lactel, Pelham, AL) were dissolved in chloroform. 400 μL of the oleic acid-coated 10 nm Fe_3O_4 nanoparticles suspension in chloroform (16.7 mg mL^{-1}) were added to the PLGA solution. To complete the oil phase of the oil-in-water emulsion, a doxorubicin solution (100 μL) was added to the PLGA–Fe_3O_4 suspension and the mixture was vortexed for complete mixing. The chloroform oil phase was then added dropwise to a water phase consisting of an aqueous solution of PVA (1.5 mL, 2% (w/v)). The PVA serves as an emulsifying agent to stabilize the oil phase in the water. The mixture was then vortexed at high speed for 3 min to create an emulsion. The emulsion was sonicated in a bath sonicator (Fisher Scientific FS30D) for 6 min to produce a more uniform emulsion, followed by gently stirring overnight with the lid off to allow the chloroform to evaporate. Finally, the solution was washed 3 times with a 100 kDa MW cut-off centrifuge filter and resuspended with water (4 mL) after the first two washes and 1 mL of water after the final wash. PLGA particles were separated using the appropriate variety of filter membranes to obtain the desired particle size fractionation.

NANO MICRO small

PDMS Channels Preparation: Polydimethylsiloxane (PDMS) was hand-mixed in a 10:1 polymer:fixing agent ratio using the commercial Sylgard 184 Silicone elastomer kit. PDMS was poured over a glass Petri dish, degassed in a vacuum desiccator, and baked at 110 °C for 15 min. Holes of ≈2 mm were punched in each well using a puncher (Ted Pella, Redding, CA). An open channel of ≈200 μm wide and ≈10 mm in length was used to properly visualize the magnetic nanowire motors. The resultant structures and cleaned glass slides were exposed to UVO ozone (Jetline Co., Irvine, CA) at a gas flow rate of 3 sccm for 5 min, pressed together and baked for another 10 min at 110 °C to complete the bonding process. The PDMS channel was washed with ultra pure water to ensure the removal of any residual dust and dried properly under nitrogen before starting the experiments. Ambient light and digital adjustments to brightness and contrast were used to visualize the magnetic nanowires with the cargo and the PDMS channel at the same time.

Magnetically Driven Movement: The magnetic field was achieved by a triaxial Helmholtz coil, consisting of a homogeneous rotating magnetic field and a constant magnetic field which is perpendicular to the axis of the rotating one (See SI Figure 1). The magnetic induction was measured using a Gaussmeter (Model 475 DSP Gaussmeter, Lake Shore Cryotronics, Inc, Westerville, OH). The magnetic nanomotors were driven by a magnetic field with an unsteady component of amplitude H_1, rotating sinusoidally in a plane perpendicular to a constant component, H_0. The magnetic field precessed about the direction of the constant magnetic field at an angular frequency $\Omega = 2\pi f$.

Cell Line and Culture: HeLa cells were cultured in a flask in RPMI medium supplemented with 10% fetal calf serum, penicillin (100 μg mL^{-1}), and streptomycin (100 μg mL^{-1}). The HeLa cells were incubated with 5% CO_2 at 37 °C until 80% confluent. The cells were treated with trypsin and centrifuged at 1000 rpm for 10 min to form a pellet. The cells were resuspended in fresh RPMI medium and counted with a hemacytometer in order to determine the cell concentration per mL. The cells were seeded in the PDMS wells attached to slide coverslips at approximately 10^4 cells cm^{-2}. The PDMS coverslips were placed inside a 100 mm cell-culture dish and an additional coverslip was placed over the PDMS well to prevent evaporation. The cells were allowed to incubate overnight and were used in subsequent experiments.

Experiments in PDMS Channels: Ni–Ag_{flex} magnetic nanowires were repeatedly washed (10 times) with culture media to remove the remaining peroxide residue. Then the PDMS channel was filled with culture media (500 μL) and an appropriate volume of the washed flexible Ni–Ag_{flex} magnetic nanowire suspension and the drug-loaded magnetic PLGA microparticles (≈10 μL of each) was added to the magnetic microparticles capture well. After capturing the magnetic microparticles, the flexible nanowires were magnetically guided across the channel to the target cells reservoir. HeLa cells were plated 24 h earlier in the corresponding reservoir selected for a stationary delivery.

Supporting Information

Supporting Information is available from the Wiley Online Library or from the author.

Acknowledgements

This work was supported by the National Science Foundation (Award Number CBET-0853375 to JW, CBET-0746285 to EL and CMMI-1031239 to LZ) and the Croucher Foundation (through a scholarship to OSP). SC acknowledges the support from Programa Becas Complutense del Amo (2010-2011). The authors would like to acknowledge also K. Chan for helping the magnetic setup and Allen Pei, Adam Ponedal for assisting in the nanowires preparation.

[1] J. Burdick, R. Laocharoensuk, P. M. Wheat, J. D. Posner, J. Wang, *J. Am. Chem. Soc.* **2008**, *130*, 8164.
[2] S. Sundararajan, P. E. Lammert, A. W. Zudans, V. H. Crespi, A. Sen, *Nano Lett.* **2008**, *8*, 1271.
[3] D. Kagan, R. Laocharoensuk, M. Zimmerman, C. Clawson, S. Balasubramanian, D. Kang, D. Bishop, S. Sattayasamitsathit, L. Zhang, J. Wang, *Small* **2010**, *6*, 2741.
[4] J. Wang, *ACS Nano* **2009**, *3*, 4.
[5] S. Sundararajan, S. Sengupta, M. E. Ibele, A. Sen, *Small* **2010**, *6*, 1479.
[6] T. Mirkovic, N. S. Zacharia, G. D. Scholes, G. A. Ozin, *ACS Nano* **2010**, *4*, 1782.
[7] Y. F. Mei, A. A. Solovev, S. Sanchez, O. G. Schmidt, *Chem. Soc. Rev.* **2011**, *40*, 2109.
[8] A. A. Solovev, S. Sanchez, M. Pumera, Y. F. Mei, O. G. Schmidt, *Adv. Funct. Mater.* **2010**, *20*, 2430.
[9] L. Zhang, K. E. Peyer, B. J. Nelson, *Lab Chip* **2010**, *10*, 2203.
[10] S. Balasubramanian, D. Kagan, C.-M. Hu, S. Campuzano, M. J. Lobo-Castañon, N. Lim, D. Y. Kang, M. Zimmerman, L. Zhang, J. Wang, *Angew. Chem. Int. Ed.* **2011**, *50*, 4161.
[11] D. Kagan, S. Campuzano, S. Salasubramanian, F. Kuralay, G. U. Flechsig, J. Wang, *Nano Lett.* **2011**, *11*, 2083.
[12] L. Zhang, J. J. Abbott, L. X. Dong, B. E. Kratochvil, D. Bell, B. J. Nelson, *Appl. Phys. Lett.* **2009**, *94*, 64107.
[13] A. Ghosh, P. Fischer, *Nano Lett.* **2009**, *9*, 2243.
[14] W. Gao, S. Sattayasamitsathit, K. M. Manesh, D. Weihs, J. Wang, *J. Am. Chem. Soc.* **2010**, *132*, 14403.
[15] W. Gao, K. M. Manesh, J. Hua, S. Sattayasamitsathit, J. Wang, *Small* **2011**, *7*, 2047.
[16] O. S. Pak, W. Gao, J. Wang, E. Lauga, *Soft Matter* **2011**, *7*, 8169.
[17] E. M. Purcell, *Am. J. Phys.* **1977**, *45*, 3.
[18] E. Lauga, T. R. Powers, *Rep. Prog. Phys.* **2009**, *72*, 096601.
[19] O. Raz, A. M. Leshansky, *Phys. Rev. E* **2008**, *77*, 055305(R).
[20] P. Tierno, O. Güell, F. Sagués, R. Golestanian, I. Pagonabarraga, *Phys. Rev. E* **2010**, *81*, 011402.
[21] P. Tierno, R. Golestanian, I. Pagonabarraga, F. Sagués, *Phys. Rev. Lett.* **2008**, *101*, 218304.
[22] W. Chaisri, W. E. Hennink, S. Okonogi, *Curr. Drug Deliv.* **2009**, *6*, 69.

Received: September 14, 2011
Published online: December 15, 2011

